Supplement of Clim. Past, 22, 675–688, 2026
https://doi.org/10.5194/cp-22-675-2026-supplement

Climate of the Past Open Access EGU

Supplement of

Simulating global ice volume across the Mid-Pleistocene Transition with a ramp-like increase in the deglaciation threshold

Felix Pollak et al.

Correspondence to: Felix Pollak (felix.pollak@univ-grenoble-alpes.fr)

S1 Changes compared to the L23 models

Several changes are made in the RAMP model compared to the L23 models to reduce the number of model parameters, increase the physical interpretability of the results, remove unnecessary parameterizations, enable other tuning targets and obtain a better performance overall.

S1.1 Parameterization

- Paillard (1998) introduced an artificial truncation function for the orbital forcing in his P98 model, which was thereafter adopted in all the successor models, including the L23 models. This adjustment was implemented to account for the ice volume being less sensitive to forcing during colder periods. For obliquity, the truncation was always applied in the L23 models, while for precession and co-precession it was only applied in the differential equations of their model (their Eq. 1,2), but not for their threshold equations (their Eq. 5,6). To remove this inconsistency from the model and rely only on the orbital parameters as input, we remove this truncation function for the new RAMP model. In addition, the P98 model used a specific insolation metric, while the RAMP model uses a linear combination of precession and obliquity. Therefore, the orbital forcing can be adjusted in the tuning process in such a way that it already incorporates specific mechanisms, like the proposed reduction in sensitivity, and it seems not necessary to include this truncation anymore. We also carried out simulations with and without a truncation function (not shown), resulting in almost the same output.

- The L23 models used a linear combination of precession, co-precession and obliquity for the orbital forcing. This approach is not new and has been used in previous models (Imbrie et al., 2011; Parrenin and Paillard, 2012). We found in our simulations that a combination of only two functions of orbital parameters is already sufficient for the model and yields almost the same output. We also tested five insolation metrics, which differ in their latitude and seasonality, and found that they can be almost perfectly reconstructed by a linear combination of just these two functions of orbital parameters (Fig. S2). Therefore, we no longer use co-precession (Eco) for the RAMP model. This reduces the model parameters and makes it easier to investigate the influence of precession and obliquity, since they are now only controlled by two parameters.

- The PP12 model first introduced the α_d parameter for the deglacial evolution, which was later adopted in the L23 models (their Eq. 2). This parameter describes the speed of the deglaciation. However, both models also include the term $-\frac{v(t)}{\tau_d}$ in their deglacial evolution. The purpose of this term is to quickly decay a large ice volume over a short amount of time. Hence, in combination with the slow glaciations, this approach was able to reproduce the typical sawtooth-like pattern of the 100 kyr world. The question arises, whether both terms are required to achieve this goal, or if the latter one is sufficient. The P98 model and the model by Leloup and Paillard (2022) (hereafter referred to as LP22) were both capable of simulating the 100 kyr world accurately, only using the $-\frac{v(t)}{\tau_d}$ term. Including the α_d parameter into the RAMP model only slightly alters the simulation outcome (not shown). Hence, it seems justified to drop this parameter for the RAMP model. Excluding this parameter from the model has another advantage, namely improving the physical interpretability of the relaxation time τ_d. Once the model switches to a deglaciation state, a large ice volume $v(t)$ can be rapidly decayed, if τ_d is small, since the term $-\frac{v(t)}{\tau_d}$ adds a large negative value to the evolutionary equation. However, as long as there is another term α_d in this equation, a large positive value of α_d can compensate for the term $-\frac{v(t)}{\tau_d}$. So, for such a parameterization, τ_d must always be considered together with the value of α_d.

- The L23 models use two different orbital forcings for their differential equations and their threshold equations. The first one $I_\alpha = \alpha_{\mathrm{Esi}}\mathrm{Esi} + \alpha_{\mathrm{Eco}}\mathrm{Eco} + \alpha_{\mathrm{O}}\mathrm{Ob}$ is defined by a set of α parameters (their Eq. 1,2) and the second one $I_k = k_{\mathrm{Esi}}\mathrm{Esi} + k_{\mathrm{Eco}}\mathrm{Eco} + k_{\mathrm{O}}\mathrm{Ob}$ by a set of k parameters (their Eq. 5,6). The necessity of relying on two different orbital forcings comes from the fact that the L23 models are not dimensionless. Parrenin and Paillard (2003) introduced in their model a threshold which depends on a combination of the orbital forcing and ice volume. The later models (PP12, LP22, L23) all used a similar approach. While the dimensionless and normalised LP22 model uses a single orbital forcing I and simply relies on $I + v$ as a threshold, this does not work for the dimensional PP12 and L23 models. The first issue is that I_α has dimensions of $\mathrm{m\,kyr^{-1}}$ and v is given in $\mathrm{m\,sl}$. Secondly, I_α and v have different orders of magnitude,

with I_α ranging between values of ± 4 and with v between 0 and 100 (for the L23 models). This means that in the late Quaternary, when the ice volume increased, the orbital forcing I_α would become negligible compared to $v(t)$. This also explains why the k parameters in the L23 models are at least an order of magnitude larger than their corresponding α values. The added k parameters in the PP12 and L23 models resolve these two issues, but add three extra parameters to the model and also introduce two orbital forcings that can differ not only in amplitude, but also in their frequencies, since the α and k parameters are selected independently. Hence, I_α and I_k can differ in their precession and obliquity signals, which is physically hard to justify. While the new RAMP model is still dimensional, we circumvent these issues by using a slightly altered threshold. Firstly, in our threshold equations (Eq. 6,7), we use the dimensionless orbital forcing $\tilde{I}$ instead of I. Secondly, we scale $\tilde{I}$ by the current ice volume $v(t)$. This assures that the scaled dimensionless orbital forcing $v \cdot \tilde{I}$ has a similar magnitude as v. This simple adjustment requires no additional parameters and removes all three k parameters for the RAMP model.

– The L23 models are three distinct model versions that differ in their temporal evolution of the deglaciation parameter $v_0(t)$. The ORB model is purely externally driven, with a constant v_0, the ABR model exhibits an abrupt change in v_0, and the GRAD model shows a gradual increase in v_0 over the entire simulation period. Legrain et al. (2023) tuned each of these simulations individually and compared the model results with each other to conclude which temporal scenario is the most likely. Instead of relying on different model versions which explicitly resemble a specific temporal evolution, we incorporate all of them into a single model, the new RAMP model. The ramp-like implementation in $v_0(t)$ (Eq. 8) includes the following temporal scenarios:

  - if $v_{0,1} = v_{0,2}$: no change in the deglaciation parameter. RAMP is only externally forced by changes in orbital parameters (equivalent to ORB model in L23)
  - if $t_1 = t_2$: abrupt jump in $v_0(t)$ (equivalent to ABR model in L23)
  - if $t_1 = -2.6$ Myr and $t_2 = 0$ Myr: gradual trend over entire simulation period (equivalent to GRAD model in L23)
  - scenarios in between with extended linear trends in $v_0(t)$, but limited during a period from t_1 to t_2

  Therefore, the new RAMP model is more flexible than any of the L23 models, and for a linear trend in v_0, it also gives information on when such a trend has started and ended. Tuning the RAMP model to some global ice volume curve reveals the temporal evolution in $v_0(t)$, needed to best reproduce this curve. So, no comparison between different model versions (e.g. GRAD vs ABR) is needed for the RAMP model, which further simplifies the interpretation of the results.

– The RAMP model has 9 model parameters: $\alpha_{\mathrm{Esi}}, \alpha_{\mathrm{O}}, \alpha_{\mathrm{g}}, \tau_d, v_{0,1}, v_{0,2}, t_1, t_2, v_1$ (excluding the initial values v_i and $\mathrm{state}_{\mathrm{initial}}$). In contrast, all the L23 model versions have more parameters (ORB (11), ABR(13), GRAD(12)), while being less flexible than the RAMP model and revealing less information on how a temporal change in v_0 could look like, since they all focus on one specific scenario.

S1.2 Model speedup

Although a single simulation run for a set of parameters is very fast ($\mathcal{O}(s)$), tuning the model to some target curve to find an optimal set of parameters can be computationally expensive and is done with some sort of Markov Chain Monte Carlo (MCMC) algorithm, which requires running the model tens to hundreds of thousands of times. To improve the speed of the model, we translated the Python source code into *JAX* (**?**), which is a Python library for accelerated array computations with just-in-time compilations. To demonstrate the increase in speed, we run both the GRAD and RAMP models for four different tuning configurations, where we vary the number of walkers for the MCMC algorithm (nwalkers), the total tuning steps (niterations) and the number of cores used (ncores). The indicated times are averages over three tuning runs. The computations were performed on a Dell Precision 5480 computer (processor: 13th Gen Intel® Core™ i7-13800H × 20, memory: 32 GiB). Table S1 shows that the gained speedup depends on the specific configuration, but it is around a factor of 30.

Table S1. Tuning times for the GRAD (Legrain et al., 2023) and the RAMP (this study) models for three different tuning configurations. The presented time is averaged over three tuning runs. Tuning was performed with the *emcee* solver.

Model	nwalkers	niterations	ncores	Tuning time	Speedup
GRAD (Legrain et al., 2023)	50	10k	20	34.5 min	34.5
RAMP (this study)				1.0 min	
GRAD (Legrain et al., 2023)	100	10k	20	51.3 min	30.2
RAMP (this study)				1.7 min	
GRAD (Legrain et al., 2023)	50	100k	20	355 min	26.6
RAMP (this study)				13.4 min	

S1.3 Improved tuning strategy

The L23 models relied on a Markov Chain Monte Carlo (MCMC) method for their parameter tuning, namely the Python package *emcee* (Foreman-Mackey et al., 2013) which implements the affine invariant ensemble sampler for Markov chain Monte Carlo algorithms, introduced by Goodman and Weare (2010). The RAMP model uses the same solver, but due to the increase in numerical efficiency, a larger number of walkers (between 100 and 1,000) and tuning iterations (typically 100,000) can be used to explore the parameter space more rigorously. Moreover, instead of using a simple *stretch move* (Goodman and Weare, 2010) as done in the L23 models, we apply a combination of different moves for the proposal function. That is, a mixture of 90% *Differential Evolution (DE)* moves and 10% *DE Snooker* moves, as suggested by Ter Braak and Vrugt (2008).

Furthermore, to verify convergence and escape possible local minima, we also use the Python package *ptemcee* (Vousden et al., 2016; Foreman-Mackey et al., 2013), which implements parallel tempering in the *emcee* framework. Here, we use 20 different temperatures for the tuning. Another sampler that we implemented is *dynesty* (Speagle, 2020; Koposov et al., 2024), which is a dynamic nested sampling package in Python. This modular approach with multiple different samplers allows for simple switching between the samplers, and the most suitable one for each new parameterization can be selected. Furthermore, the results of different solvers can be compared to verify convergence.

The Log-Likelihood function for the optimization is defined as:

$$\ln \mathcal{L} = -\frac{1}{2} \sum_{i=1}^{N} \left(\frac{\hat{y}_i - y_i}{\sigma} \right)^2, \tag{S1}$$

where $\hat{y}$ is the reconstructed ice volume, y the target ice volume and σ its corresponding standard deviation.

S1.4 Simulation time

The L23 models could only be run for a fixed period of time, namely, the past 2 Ma. To consider the entire Quaternary climate, the RAMP model is run by default for the past 2.6 Ma. By including a new model variable, the simulation time for the RAMP model can be easily adjusted to any period for the last 3.6 Ma. Furthermore, it can be simulated into the future to investigate the next glacial cycles in the model. These future projections do not account for anthropogenic CO_2 emissions and hence only present baseline experiments on how the climate would evolve in the absence of anthropogenic impacts.

S2 Model improvements

Table S2 presents a comparison of the RMSEs for the three distinct model configurations, as detailed in Legrain et al. (2023), against the results obtained with the new RAMP model presented in this study. The RAMP model improves the previously best-performing GRAD model by Legrain et al. (2023) by over 1 m in RMSE, while relying on 3 parameters less. The simulated curves are shown in Fig. S1.

Table S2. RAMP model (this study) compared to the L23 model versions (Legrain et al., 2023). All models are run for 2 Myr and tuned to the GMSL reconstruction by Berends et al. (2021).

Model	**Model parameters** (excl. v_i and $\text{state}_{\text{initial}}$)	**RMSE**	**Δ RMSE** (wrt RAMP model)
RAMP (this study)	9	12.8 m	NA
ORB (Legrain et al., 2023)	11	18.1 m	5.3 m
ABR (Legrain et al., 2023)	13	14.4 m	1.6 m
GRAD (Legrain et al., 2023)	12	13.9 m	1.1 m

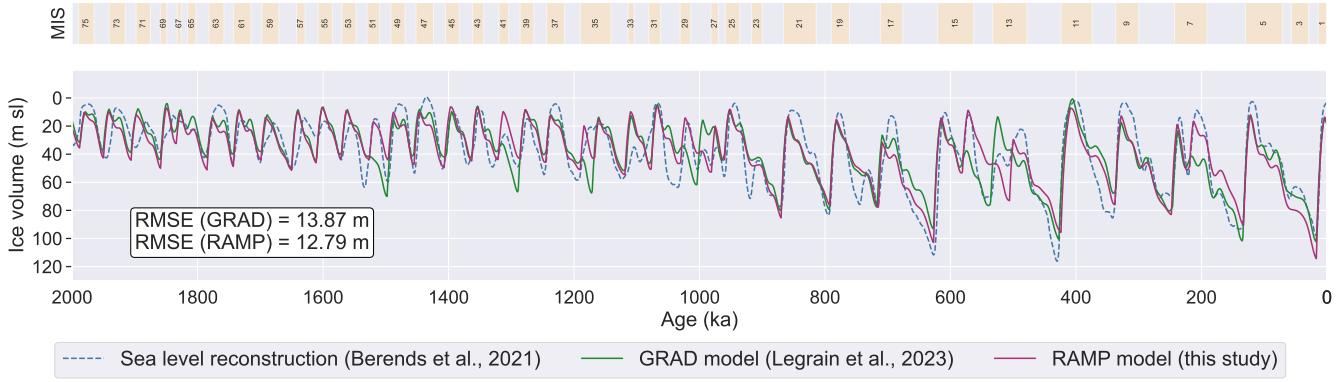

Figure S1. Comparison of GRAD model (Legrain et al., 2023) and RAMP model (this study). Both models were tuned to the GMSL reconstruction by Berends et al. (2021). MIS boundaries are given according to Lisiecki and Raymo (2005).

S3 Tuned parameters

The tuned parameter values for the RAMP model can be found in Table S3.

Table S3. Tuned parameter values of the RAMP model for the two different tuning targets used in this study. The targets are: GMSL reconstruction by Berends et al. (2021) and GMSL reconstruction by Rohling et al. (2022). $\text{state}_{\text{initial}}$ sets the initial state in which the model starts the simulation. This parameter was not used as a tunable parameter, instead, it was always set to glacial mode.

Model Target	**RAMP** Berends GMSL	**RAMP** Rohling GMSL
α_{Esi} (m kyr^{-1})	-0.54	-0.58
α_{O} (m kyr^{-1})	0.46	0.54
α_{g} (m kyr^{-1})	0.77	0.77
τ_d (kyr)	6.9	7.2
$v_{0,1}$ (m)	-0.34	-0.87
$v_{0,2}$ (m)	125.1	144.6
v_1 (m)	12.7	17.1
t_1 (kyr)	-2291	-2596
t_2 (kyr)	-546	-252
v_i (m)	27.1	27.6
$\text{state}_{\text{initial}}$	glacial	glacial
# Parameters (excluding v_i and $\text{state}_{\text{initial}}$)	9	9

S4 Linear combination of two functions of orbital parameters

To demonstrate that even two functions of orbital parameters (precession parameter and obliquity) can almost perfectly reconstruct various insolation curves, we show this for five exemplary insolation curves (see Fig. S2). Insolation (I), precession (Esi) and obliquity (Ob) values are taken from Laskar et al. (2004) and were normalised. ISI computation was carried out with code from Leloup and Paillard (2022). $I_{aprox} = \alpha_{Esi}\mathrm{Esi} + \alpha_{\mathrm{O}}\mathrm{Ob}$ is the linear combination. We find the following solutions for these five orbital forcings:

- I_{SS}^{65N}: Insolation at 65° N on 21st June: $\alpha_{\mathrm{Esi}} = -0.917,\ \alpha_{\mathrm{O}} = 0.393$
- I_{WS}^{65N}: Insolation at 65° N on 21st December: $\alpha_{\mathrm{Esi}} = 0.093,\ \alpha_{\mathrm{O}} = -0.991$
- I_{SS}^{Eq}: Insolation at the Equator on 21st June: $\alpha_{\mathrm{Esi}} = -0.995,\ \alpha_{\mathrm{O}} = -0.094$
- I_{WS}^{90S}: Insolation at 90° S on 21st December: $\alpha_{\mathrm{Esi}} = 0.892,\ \alpha_{\mathrm{O}} = 0.451$
- ISI$(\tau = 300)_{65N}$: ISI above 300 W/m^2 at 65° N: $\alpha_{\mathrm{Esi}} = -0.523,\ \alpha_{\mathrm{O}} = 0.850$

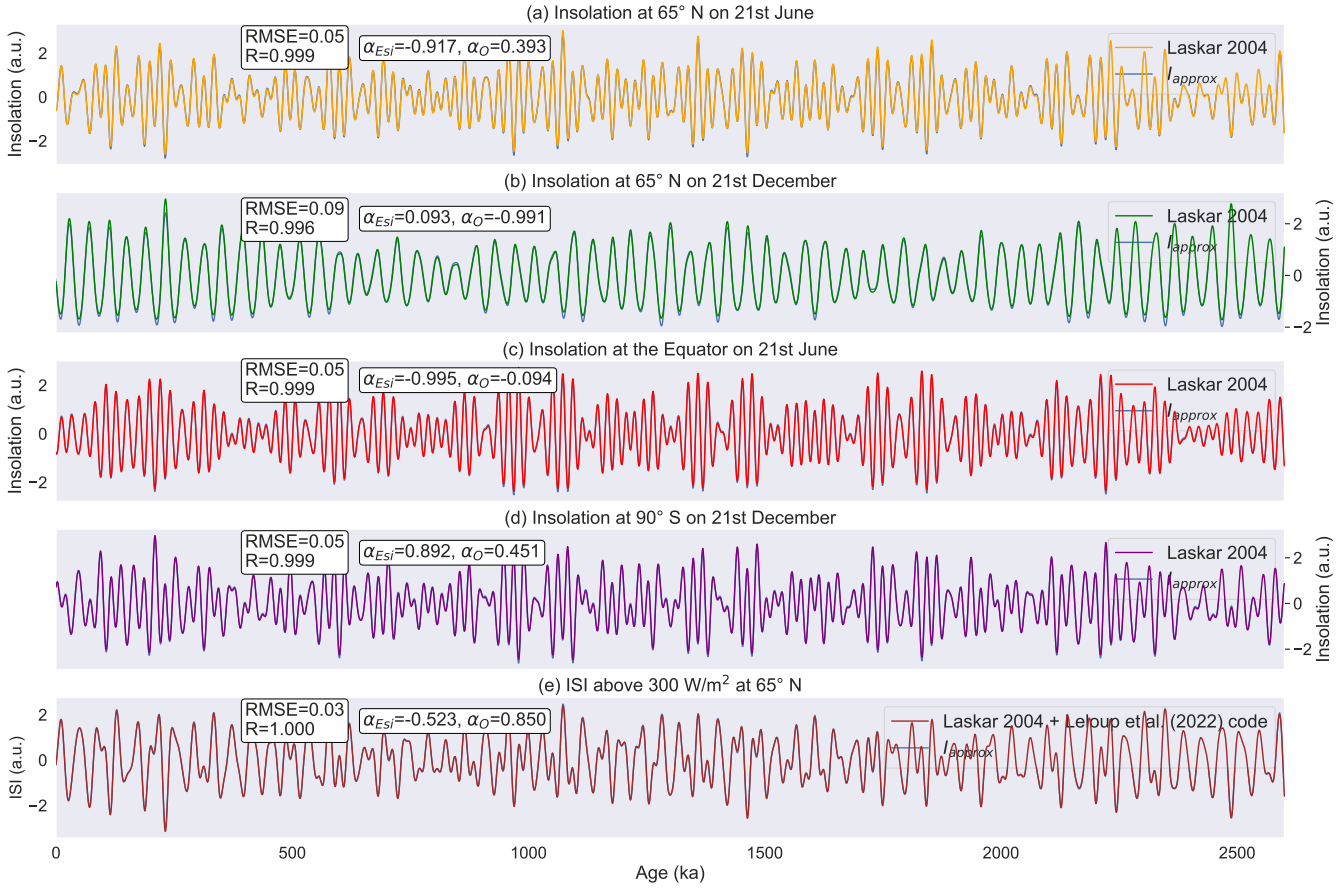

Figure S2. Various insolation curves from Laskar et al. (2004). ISI computations were carried out with code from Leloup and Paillard (2022). I_{approx} is the corresponding best linear approximation, based on a linear combination of the precession parameter (Esi) and obliquity (Ob): $I_{approx} = \alpha_{\mathrm{Esi}}\mathrm{Esi} + \alpha_{\mathrm{O}}\mathrm{Ob}$.

S5 State thresholds in the RAMP model

Figure S3 visualizes how the 2-state approach in the RAMP model (for Berends GMSL target) works in combination with the two threshold equations (Eq. 6,7), needed for state transitions. It depicts the period 1.2 - 0.6 Ma, when the RAMP model produces an almost abrupt change in the amplitude and frequency of glacial cycles. Firstly, it can be seen that the deglaciation parameter $v_0(t)$ (black dotted line) increases linearly during this period. The red-shaded areas indicate when the scaled orbital forcing $v \cdot \tilde{I}$ (red line) is above the model threshold v_1, and the blue-shaded areas mark the periods when it is below this threshold. Due to the definition of the threshold $v \cdot \tilde{I} + v \gtrless v_0$, the scaled forcing effectively lowers the deglaciation threshold in periods of large forcing and increases it during periods of lower forcing. As outlined in the Methods section, two conditions must be met to trigger a deglaciation (Eq. 6) and two conditions for the onset of a new glaciation (Eq. 7). A termination is triggered once the ice volume exceeds the effective deglaciation threshold and the scaled forcing is above the v_1 threshold. Once both conditions are met (purple dots), a state change from a glaciation to a deglaciation mode is performed, and the dynamics of the system follow Eq. (5). This is the case until two criteria are fulfilled: Firstly, the ice volume falls again below the effective deglaciation threshold (black line), and secondly, the scaled orbital forcing is smaller than the model threshold v_1 (blue-shaded area). This allows the model to enter the next glacial state (green dots), and its evolution follows Eq. (4).

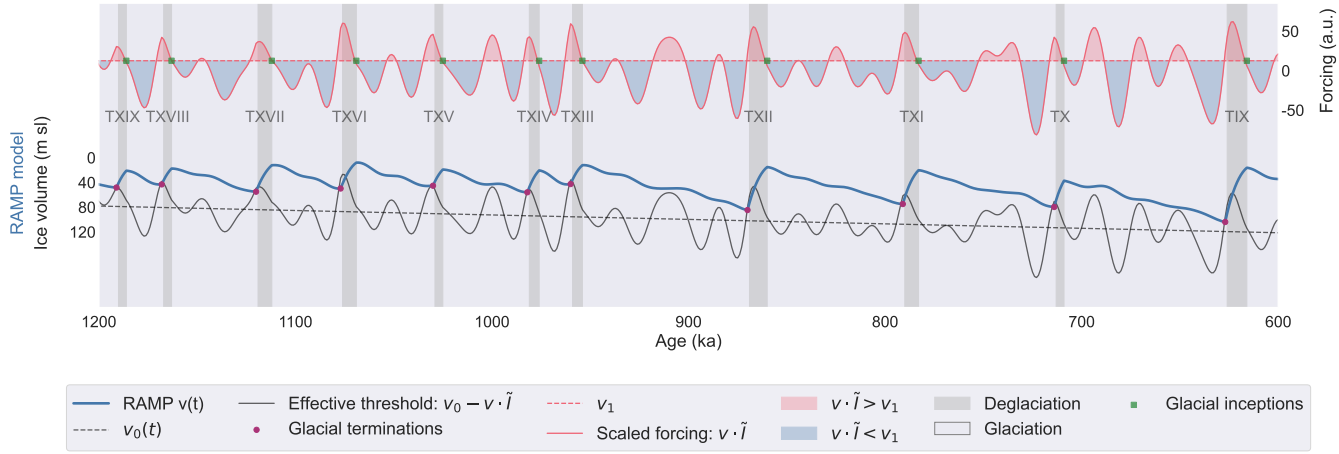

Figure S3. Visualization of state thresholds in the RAMP model. Simulated ice volume by the RAMP model (blue line) for the period 1.2 - 0.6 Ma, together with its deglaciation and glaciation thresholds. The scaled orbital forcing $v \cdot \tilde{I}$ is shown in red. While the red shaded area marks values above the model threshold v_1, the blue shaded area marks values below. The time-dependent deglaciation parameter $v_0(t)$ is represented by the black dotted line, while the solid black line indicates the effective deglaciation threshold ($v_0 - v \cdot \tilde{I}$). The purple dots indicate terminations, and the red dots mark glacial inceptions. Modelled terminations are labelled with Roman numerals.

S6 Tested parameterizations

Due to the increase in model speed and an improved tuning strategy, we could test various parameterizations in the model to test the impact of various parameters in the model. A selection of some tested parameterizations can be found in Table S4. This process allowed us to identify the importance of scaling the orbital forcing $I(t)$ with the ice volume $v(t)$ in the threshold equations and come up with the final version of the RAMP model, as described in the main manuscript.

Table S4. Selection of tested parameterizations, to come up with a final version of the RAMP model. Changes have been made to the orbital forcing (I or I_α). Some of the parameterizations used a second orbital forcing, I_k, for the threshold equations, as has been done for the L23 models. Model parameterizations which rely on a single orbital forcing contain the entry $I_k = I$.

Model	# Params (excl. v_i, $\text{state}_{\text{initial}}$)	Note	Forcing I_α	Forcing I_k	$\frac{dv}{dt} =$	Deglaciation threshold	Glaciation threshold	Berends GMSL (2.6 Myr) RMSE (m)
RAMP41	9	- droppped α_d - τ_d = const. - dropped Eco - units of I (m/ka) and v (m) don't match	$I = \alpha_{\text{Esi}}\text{Esi} + \alpha_{\text{O}}\text{Ob}$	$I_k = I$	$\frac{dv}{dt} = -I + \ldots$	(i) $I + v > v_0$ (ii) $I > v_1$	(i) $I + v < v_0$ (ii) $I < v_1$	13.91
RAMP42	11	- based on RAMP41 - added l parameters to I_k	$I_\alpha = \alpha_{\text{Esi}}\text{Esi} + \alpha_{\text{O}}\text{Ob}$	$I_k = I_\alpha + l_{\text{Esi}} \cdot v\text{Esi} + l_{\text{O}} \cdot v\text{Ob}$	$\frac{dv}{dt} = -I_\alpha + \ldots$	(i) $I_k + v > v_0$ (ii) $I_k > v_1$	(i) $I_k + v < v_0$ (ii) $I_k < v_1$	11.79
RAMP43	11	- based on RAMP41 - added l parameters to both I - units of I (m/ka) and v (m) don't match	$I = \alpha_{\text{Esi}}\text{Esi} + \alpha_{\text{O}}\text{Ob} + l \cdot v(\text{Esi} + \text{Ob})$	$I_k = I$	$\frac{dv}{dt} = -I + \ldots$	(i) $I + v > v_0$ (ii) $I > v_1$	(i) $I + v < v_0$ (ii) $I < v_1$	12.94
RAMP46	10	- based on RAMP41 - added new τ parameter for correct units	$I = \alpha_{\text{Esi}}\text{Esi} + \alpha_{\text{O}}\text{Ob}$	$I_k = I$	$\frac{dv}{dt} = -\frac{I}{\tau} + \ldots$	(i) $I + v > v_0$ (ii) $I > v_1$	(i) $I + v < v_0$ (ii) $I < v_1$	12.81
RAMP49	12	- based on RAMP46 - added l parameters to both I	$I = \alpha_{\text{Esi}}\text{Esi} + \alpha_{\text{O}}\text{Ob} + l_{\text{Esi}} \cdot v\text{Esi} + l_{\text{O}} \cdot v\text{Ob}$	$I_k = I$	$\frac{dv}{dt} = -\frac{I}{\tau} + \ldots$	(i) $I + v > v_0$ (ii) $I > v_1$	(i) $I + v < v_0$ (ii) $I < v_1$	12.03
RAMP50	12	- based on RAMP46 - added l parameters only to I_k	$I_\alpha = \alpha_{\text{Esi}}\text{Esi} + \alpha_{\text{O}}\text{Ob}$	$I_k = I_\alpha + l_{\text{Esi}} \cdot v\text{Esi} + l_{\text{O}} \cdot v\text{Ob}$	$\frac{dv}{dt} = -\frac{I_k}{\tau} + \ldots$	(i) $I_k + v > v_0$ (ii) $I_k > v_1$	(i) $I_k + v < v_0$ (ii) $I_k < v_1$	11.74
RAMP53	11	- based on RAMP46 - added one l parameter to I_k	$I_\alpha = \alpha_{\text{Esi}}\text{Esi} + \alpha_{\text{O}}\text{Ob}$	$I_k = I_\alpha + l \cdot v(\text{Esi} + \text{Ob})$	$\frac{dv}{dt} = -\frac{I_k}{\tau} + \ldots$	(i) $I_k + v > v_0$ (ii) $I_k > v_1$	(i) $I_k + v < v_0$ (ii) $I_k < v_1$	11.83
RAMP57	11	- based on RAMP46 - added one l parameter to both I	$I = \alpha_{\text{Esi}}\text{Esi} + \alpha_{\text{O}}\text{Ob} + l \cdot v(\text{Esi} + \text{Ob})$	$I_k = I$	$\frac{dv}{dt} = -\frac{I}{\tau} + \ldots$	(i) $I + v > v_0$ (ii) $I > v_1$	(i) $I + v < v_0$ (ii) $I < v_1$	12.07
RAMP66	10	- no τ parameter - same I, but changed threshold	$I = \alpha_{\text{Esi}}\text{Esi} + \alpha_{\text{O}}\text{Ob}$	$I_k = I$	$\frac{dv}{dt} = -I + \ldots$	(i) $l \cdot v \cdot (\text{Esi} + \text{Eco}) + v > v_0$ (ii) $l \cdot v \cdot (\text{Esi} + \text{Eco}) > v_1$	(i) $l \cdot v \cdot (\text{Esi} + \text{Eco}) + v < v_0$ (ii) $l \cdot v \cdot (\text{Esi} + \text{Eco}) < v_1$	11.89
RAMP67	9	- based on RAMP66, but no more l parameter	$I = \alpha_{\text{Esi}}\text{Esi} + \alpha_{\text{O}}\text{Ob}$	$I_k = I$	$\frac{dv}{dt} = -I + \ldots$	(i) $v \cdot (\text{Esi} + \text{Eco}) + v > v_0$ (ii) $v \cdot (\text{Esi} + \text{Eco}) > v_1$	(i) $v \cdot (\text{Esi} + \text{Eco}) + v < v_0$ (ii) $v \cdot (\text{Esi} + \text{Eco}) < v_1$	12.10
RAMP71	10	- based on RAMP66, but changed sign of Esi in threshold	$I = \alpha_{\text{Esi}}\text{Esi} + \alpha_{\text{O}}\text{Ob}$	$I_k = I$	$\frac{dv}{dt} = -I + \ldots$	(i) $l \cdot v \cdot (-\text{Esi} + \text{Eco}) + v > v_0$ (ii) $l \cdot v \cdot (-\text{Esi} + \text{Eco}) > v_1$	(i) $l \cdot v \cdot (-\text{Esi} + \text{Eco}) + v < v_0$ (ii) $l \cdot v \cdot (-\text{Esi} + \text{Eco}) < v_1$	15.07
RAMP72	9	- based on RAMP67, but changed second threshold	$I = \alpha_{\text{Esi}}\text{Esi} + \alpha_{\text{O}}\text{Ob}$	$I_k = I$	$\frac{dv}{dt} = -I + \ldots$	(i) $v \cdot (\text{Esi} + \text{Eco}) + v > v_0$ (ii) $I > v_1$	(i) $v \cdot (\text{Esi} + \text{Eco}) + v < v_0$ (ii) $I < v_1$	13.28

S7 RAMP-2 model

The RAMP model (as well as its precursor models: P98, PP12, LP22, L23) all rely on an increasing value in v_0. This increase in v_0 was initially proposed by Paillard (1998) in his conceptual model and adopted in later models (PP12 by Parrenin and Paillard (2012), LP22 by Leloup and Paillard (2022), L23 by Legrain et al. (2023)) to simulate an increase in ice volume over the Pleistocene. This increase in global ice volume stems from the used target curves, namely some benthic δ^{18}O record, like LR04, or the GMSL reconstruction by Berends et al. (2021). However, the new GMSL curve by Clark et al. (2025) is structurally completely different to former reconstructions, such as the Berends curve, since it no longer shows an increase in amplitude, but just in frequency. The model design of the RAMP model is less suited for such a target curve since it was specifically designed to simulate an increase in global ice volume. We tested various parameterizations (of the RAMP model) in order to reconstruct the new GMSL by Clark et al. (2025) and found that if the glaciation threshold of the RAMP model is slightly altered, this new model (which we call RAMP-2) is capable of reconstructing the Clark GMSL curve, especially it is capable of simulating the shift in frequency without an increase in amplitude. Simultaneously, the RAMP-2 model can still reconstruct the Berends GMSL if tuned onto this target. The new parameterization and the results are discussed below.

Parameterization

The RAMP-2 model is only altered in its threshold equations, the remaining parameterizations stay the same. A state change from a glaciation to a deglaciation (**g**) $\rightarrow$ (**d**) occurs when a combination of the current ice volume $v(t)$ and the orbital forcing exceeds a critical threshold:

$$v(t) \cdot \tilde{I}(t) + v(t) > v_0(t). \tag{S2}$$

Vice versa, a transition from a deglaciation to a glaciation state (**d**) $\rightarrow$ (**g**) occurs when:

$$\text{(i)} \quad I(t) < I_0(t) \qquad \& \qquad \text{(ii)} \quad v(t) < v_1(t). \tag{S3}$$

The threshold parameters $v_0(t)$, $v_1(t)$ and $I_0(t)$ change ramp-like between t_1 and t_2:

$$x(t) = \begin{cases} x_1, \\ x_1 + \dfrac{x_2 - x_1}{t_2 - t_1}(t - t_1), \\ x_2, \end{cases} \qquad \begin{cases} \text{if } t < t_1 \\ \text{if } t_1 \leq t \leq t_2, \\ \text{if } t_2 < t \end{cases} \tag{S4}$$

with $x \in \{v_0, v_1, I_0\}$, $x_1 \in \{v_{0,1}, v_{1,1}, I_{0,1}\}$ and $x_2 \in \{v_{0,2}, v_{1,2}, I_{0,2}\}$. The RAMP-2 model has three more parameters than the RAMP model, leading to a total of 12 parameters (excluding v_i).

Model parameters

The tuned parameter values for the RAMP-2 model for the two different tuning targets can be found in Table S5.

Model results

The performance of the RAMP-2 model can be seen in Fig. S4, when tuned to the Berends GMSL (Fig. S4b) or the new Clark GMSL (Fig. S4c). The associated scalograms can be seen in Fig. S5. For both targets, the RAMP-2 model can reconstruct the transition towards a 100-kyr periodicity.

The RAMP-2 model presents an adjusted version of the RAMP model. It can simultaneously reconstruct the Berends and Clark GMSL. The ramp-like increase in v_0 is needed in order to simulate the increase in ice volume amplitude during the MPT, seen in the Berends GMSL. Since the Clark GMSL curve no longer exhibits an increase in amplitude, but just in frequency, an ideal model whose main goal is the reconstruction of the Clark GMSL would no longer require an increasing parameterization for the v_0 parameter. Hence, a specifically designed model for the Clark GMSL would require a different parameterization than the RAMP or RAMP-2 models.

Table S5. Tuned parameter values of the RAMP-2 model. The two different tuning targets are: GMSL reconstruction by Berends et al. (2021) and GMSL reconstruction by Clark et al. (2025). $\text{state}_{\text{initial}}$ sets the initial state in which the model starts the simulation. This parameter was not used as a tunable parameter, instead, it was always set to glacial mode.

Model Target	**RAMP-2** Berends GMSL	**RAMP-2** Clark GMSL
α_{Esi} (m kyr^{-1})	-0.51	-1.1
α_{O} (m kyr^{-1})	0.45	1.3
α_{g} (m kyr^{-1})	0.98	1.7
τ_d (kyr)	10.7	6.6
$v_{0,1}$ (m)	37.4	187
$v_{0,2}$ (m)	132	228
$v_{1,1}$ (m)	7.9	50.9
$v_{1,2}$ (m)	16.3	102.9
$I_{0,1}$ (m kyr^{-1})	-0.83	26.0
$I_{0,2}$ (m kyr^{-1})	200	-0.52
t_1 (kyr)	-2179	-2206
t_2 (kyr)	-464	-762
v_i (m)	27.4	19.7
$\text{state}_{\text{initial}}$	glacial	glacial
# Parameters (excluding v_i and $\text{state}_{\text{initial}}$)	12	12

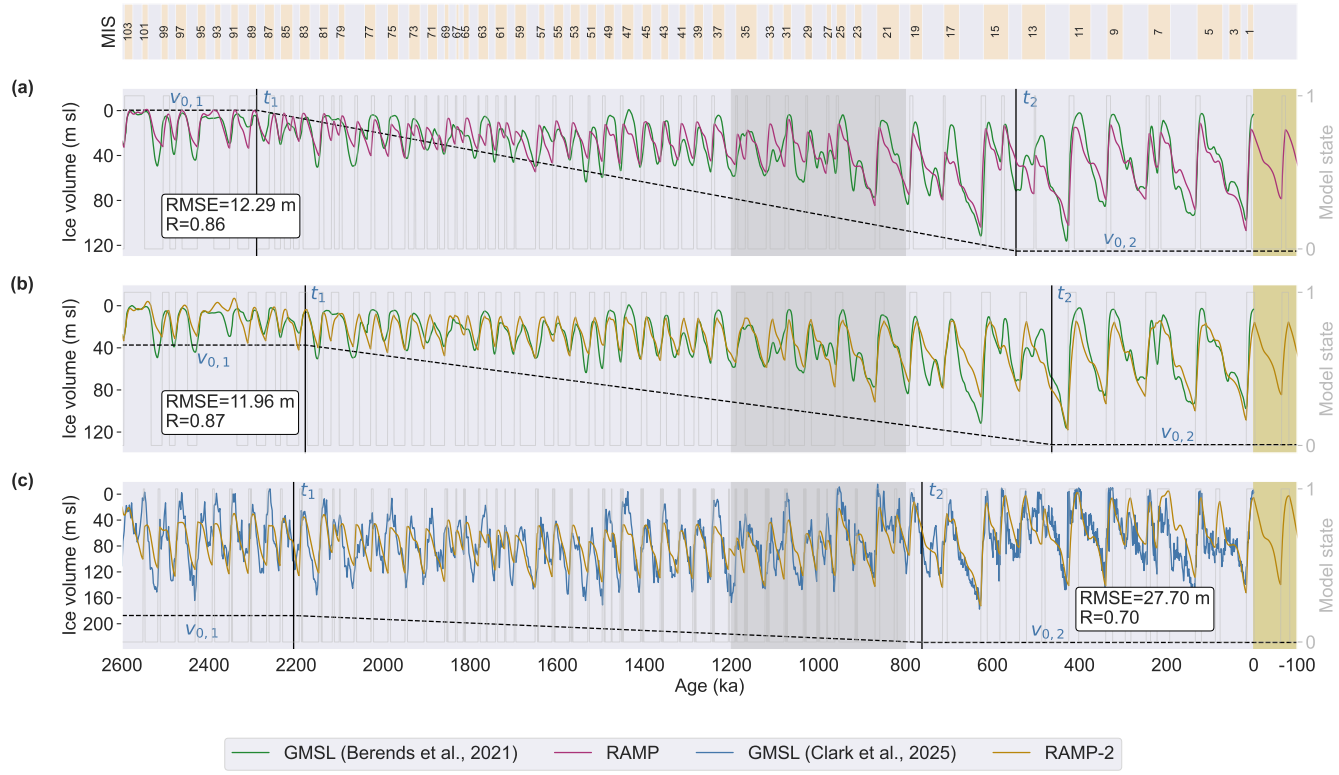

Figure S4. Comparison of the RAMP and RAMP-2 models. **(a)** The RAMP model (purple line) tuned for the Berends et al. (2021) GMSL curve. The RAMP-2 model (golden line) when **(b)** tuned for the Berends et al. (2021) GMSL curve and **(c)** for the Clark et al. (2025) GMSL curve. The vertical black lines indicate the start and endpoint of the ramp and the dotted black lines show the temporal evolution of the deglaciation threshold. The grey-shaded area highlights the classical perspective of where the MPT is located in time. MIS boundaries are given according to Lisiecki and Raymo (2005). Simulations of the future 100 kyr are indicated by the yellow-shaded areas.

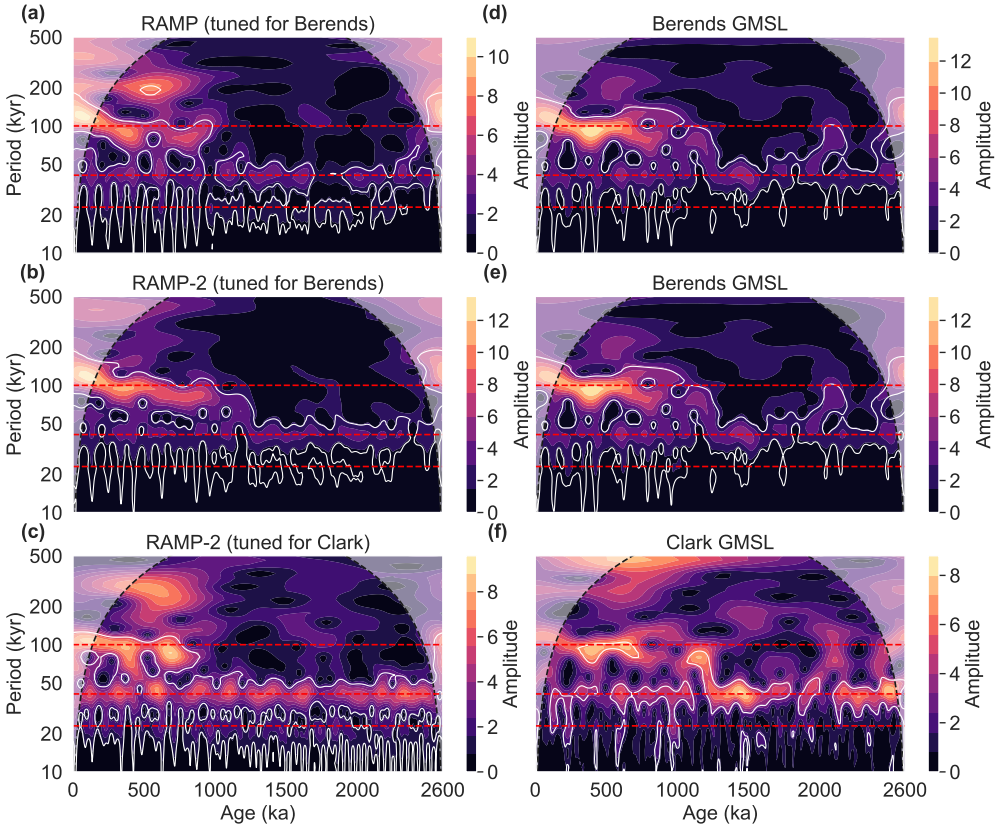

Figure S5. Frequency scalograms from the continuous wavelet transform for the RAMP **(a)** and the RAMP-2 models **(b)**, **(c)**. The scalograms of the corresponding tuning targets are: **(d)**, **(e)** Berends et al. (2021) GMSL curve and **(f)** Clark et al. (2025) GMSL curve. White contours denote significant regions above the red-noise (AR1) background at the 95% confidence level. Orbital frequencies of precession (∼23 kyr), obliquity (∼41 kyr) and eccentricity (∼100 kyr) are marked by the red dotted lines.

References

Berends, C. J., de Boer, B., and van de Wal, R. S. W.: Reconstructing the evolution of ice sheets, sea level, and atmospheric CO_2 during the past 3.6 million years, Climate of the Past, 17, 361–377, https://doi.org/10.5194/cp-17-361-2021, 2021.

Clark, P. U., Shakun, J. D., Rosenthal, Y., Pollard, D., Hostetler, S. W., Köhler, P., Bartlein, P. J., Gregory, J. M., Zhu, C., Schrag, D. P., Liu, Z., and Pisias, N. G.: Global mean sea level over the past 4.5 million years, Science, 390, https://doi.org/10.1126/science.adv8389, 2025.

Foreman-Mackey, D., Hogg, D. W., Lang, D., and Goodman, J.: emcee: The MCMC Hammer, Publications of the Astronomical Society of the Pacific, 125, 306–312, https://doi.org/10.1086/670067, arXiv:1202.3665 [astro-ph, physics:physics, stat], 2013.

Goodman, J. and Weare, J.: Ensemble samplers with affine invariance, Communications in Applied Mathematics and Computational Science, 5, 65–80, https://doi.org/10.2140/camcos.2010.5.65, 2010.

Imbrie, J. Z., Imbrie-Moore, A., and Lisiecki, L. E.: A phase-space model for Pleistocene ice volume, Earth and Planetary Science Letters, 307, 94–102, https://doi.org/10.1016/j.epsl.2011.04.018, arXiv:1104.3610 [astro-ph, physics:physics], 2011.

Koposov, S., Speagle, J., Barbary, K., Ashton, G., Bennett, E., Buchner, J., Scheffler, C., Cook, B., Talbot, C., Guillochon, J., Cubillos, P., Ramos, A. A., Dartiailh, M., Ilya, Tollerud, E., Lang, D., Johnson, B., jtmendel, Higson, E., Vandal, T., Daylan, T., Angus, R., patelR, Cargile, P., Sheehan, P., Pitkin, M., Kirk, M., Leja, J., joezuntz, and Goldstein, D.: joshspeagle/dynesty: v2.1.4, Zenodo [code], https://doi.org/10.5281/zenodo.12537467, 2024.

Legrain, E., Parrenin, F., and Capron, E.: A gradual change is more likely to have caused the Mid-Pleistocene Transition than an abrupt event, Communications Earth & Environment, 4, https://doi.org/10.1038/s43247-023-00754-0, 2023.

Leloup, G. and Paillard, D.: Influence of the choice of insolation forcing on the results of a conceptual glacial cycle model, Climate of the Past, 18, 547–558, https://doi.org/10.5194/cp-18-547-2022, 2022.

Lisiecki, L. E. and Raymo, M. E.: A Pliocene-Pleistocene stack of 57 globally distributed benthic δ18O records, Paleoceanography, 20, https://doi.org/10.1029/2004PA001071, 2005.

Paillard, D.: The timing of Pleistocene glaciations from a simple multiple-state climate model, Nature, 391, 378–381, https://doi.org/10.1038/34891, 1998.

Parrenin, F. and Paillard, D.: Amplitude and phase of glacial cycles from a conceptual model, Earth and Planetary Science Letters, 214, 243–250, https://doi.org/10.1016/S0012-821X(03)00363-7, 2003.

Parrenin, F. and Paillard, D.: Terminations VI and VIII ($\sim$ 530 and $\sim$ 720 kyr BP) tell us the importance of obliquity and precession in the triggering of deglaciations, Climate of the Past, 8, 2031–2037, https://doi.org/10.5194/cp-8-2031-2012, 2012.

Rohling, E. J., Foster, G. L., Gernon, T. M., Grant, K. M., Heslop, D., Hibbert, F. D., Roberts, A. P., and Yu, J.: Comparison and Synthesis of Sea-Level and Deep-Sea Temperature Variations Over the Past 40 Million Years, Reviews of Geophysics, 60, https://doi.org/10.1029/2022RG000775, 2022.

Speagle, J. S.: DYNESTY: a dynamic nested sampling package for estimating Bayesian posteriors and evidences, Monthly Notices of the Royal Astronomical Society, 493, 3132–3158, https://doi.org/10.1093/mnras/staa278, 2020.

Ter Braak, C. J. F. and Vrugt, J. A.: Differential Evolution Markov Chain with snooker updater and fewer chains, Statistics and Computing, 18, 435–446, https://doi.org/10.1007/s11222-008-9104-9, 2008.

Vousden, W., Farr, W. M., and Mandel, I.: Dynamic temperature selection for parallel-tempering in Markov chain Monte Carlo simulations, Monthly Notices of the Royal Astronomical Society, 455, 1919–1937, https://doi.org/10.1093/mnras/stv2422, arXiv:1501.05823 [astro-ph], 2016.